Dzyaloshinskii-Moriya interaction and spin-orbit torque at the Ir/Co interface

Yuto Ishikuro,[1] Masashi Kawaguchi,[1] Naoaki Kato,[1] Yong-Chang Lau,[1,2] and Masamitsu Hayashi[1,2,*]
[1]*Department of Physics, The University of Tokyo, Bunkyo, Tokyo 113-0033, Japan*
[2]*National Institute for Materials Science, Tsukuba 305-0047, Japan*

(Received 10 January 2019; revised manuscript received 12 March 2019; published 15 April 2019)

We studied the spin torque efficiency and the Dzyaloshinskii-Moriya interaction (DMI) of heterostructures that contain interface(s) of Ir and Co. The current-induced shifts of the anomalous Hall loops were used to determine the spin torque efficiency and DMI of [Pt/Co/X] multilayers (X = Ir, Cu) as well as Ir/Co and Pt/Ir/Co reference films. We find the effective spin Hall angle and the spin-diffusion length of Ir to be ∼0.01 and less than ∼1 nm, respectively. The short spin-diffusion length and the high conductivity make Ir an efficient spin sink layer. Such spin sink layer can be used to control the flow of spin current in heterostructures and to induce sufficient spin-orbit torque on the magnetic layer. The DMI of the Ir and Co interface is found to be in the range of ∼1.4 to ∼ 2.2 mJ/m^2, similar in magnitude to that of the Pt and Co interface. The Ir/Co and Pt/Co interfaces possess the same sign of DMI, resulting in a reduced DMI for the [Pt/Co/Ir] multilayers compared to that of the [Pt/Co/Cu] multilayers. These results show the unique role that the Ir layer plays in defining spin-orbit torque and chiral magnetism in thin-film heterostructures.

DOI: 10.1103/PhysRevB.99.134421

I. INTRODUCTION

The Dzyaloshinskii-Moriya interaction (DMI) emerges at interfaces between heavy-metal (HM) and ferromagnetic-metal (FM) layers and stabilizes chiral magnetic textures [1–3]. Chiral domain walls [4–7] and magnetic skyrmions [8–11] have been observed in systems with large DMI. In particular, the Pt/Co interface [4,5,8–11] is used as a platform to study the static and dynamic properties of chiral magnetic textures owing to its large DMI.

The sign (i.e., chirality) and strength of interfacial DMI depend on the combination of materials. Although the exact microscopic origin [12–15] of the interfacial DMI remains to be identified, significant effort has been placed to develop heterostructures with large DMI. For example, the overall DMI of the system can be increased by sandwiching a FM layer with HM layers that induce opposite magnetic chirality. Typical examples of such structures are films that consist of Pt, Co, and Ir. Experimental results [16,17] and calculations [13,14,18] suggest that the magnetic chirality at the Ir/Co interface is opposite to that of the Pt/Co interface (i.e., the magnetic chirality of Pt/Co and Co/Ir interfaces are the same). Additive and large DMI has been observed in Pt/Co/Ir multilayers in which skyrmions are stabilized [8]. Interestingly, however, experiments using magnetic domain walls indicated that the magnetic chirality of the Ir/Co interface is the same as that of the Pt/Co interface [19,20]. The DMI at the Ir/Co interface thus seems to depend on factors that are yet to be determined. Moreover, in order to electrically control the dynamics of chiral domain walls and skyrmions, it is essential to gain a solid understanding of the spin-orbit torque [21–23] (SOT) that drives the chiral magnetic structures.

Here, we study the DMI and SOT in $[Pt/Co/Ir]_N$ multilayers using measurements of the current-induced shift of the anomalous Hall loops [24]. The multilayer stack $[Pt/Co/Ir]_N$ is used since it allows increase in the thermal stability of chiral domain walls and skyrmions via increase in their magnetic volume, which is beneficial for technological applications. We compare the results of $[Pt/Co/Ir]_N$ multilayers with $[Pt/Co/Cu]_N$ multilayers (Cu replacing Ir) to reveal the role that the Ir layer plays in defining the DMI and SOT.

II. SAMPLE PREPARATION AND EXPERIMENTAL SETUP

Films were grown on Si (100) substrates, coated with 100-nm-thick silicon oxide, using magnetron sputtering. Multilayer structures are composed of Sub./3 Ta/2 Pt/[0.6 Pt/0.9 Co/d X]$_N$/2 MgO/1 Ta (units in nanometer) with X = Ir or Cu. N represents the number of repeats of the unit structure enclosed by the square brackets. X = Ir, N = 3 is referred to as film A, X = Cu, N = 3 is film B, and X = Ir, N = 1 is film C. The thickness ($0.1 \leqslant d \leqslant 1.1$ nm) of X was varied using a moving shutter during the deposition process. Three reference films were made to characterize the transport properties of Ir and the interface state of Ir/Co: film D: Sub./1.5 Ta/d Ir/1 CoFeB/2 MgO/1 Ta; film E: Sub./1.5 Ta/7 Ir/0.9 Co/2 MgO/1 Ta; and film F: Sub./3 Ta/2 Pt/1 Ir/0.9 Co/2 MgO/1 Ta. The thickness of the Ir underlayer in reference film D was varied to determine the spin-diffusion length of Ir via spin Hall magnetoresistance (SMR) [25–28] measurements. We use CoFeB as the ferromagnetic layer for the SMR measurements as it has been shown recently that an anomalously large SMR emerges in bilayers with thick Co [29]. Reference films E and F are used to study the effect, if any, of the seed layer of Ir on DMI and SOT at the Ir/Co interface: Ir is grown on a highly textured Pt(111) [30] surface for reference film F, whereas the seed layer of Ir for films A–C

*hayashi@phys.s.u-tokyo.ac.jp

TABLE I. Summary of the film ID and structure.

ID	Stack	Note
A	Sub./3 Ta/2 Pt/[0.6 Pt/0.9 Co/d Ir]$_3$/2 MgO/1 Ta	$d\sim$0.1–1.1 nm (wedge)
B	Sub./3 Ta/2 Pt/[0.6 Pt/0.9 Co/d Cu]$_3$/2 MgO/1 Ta	$d\sim$0.1–1.1 nm (wedge)
C	Sub./3 Ta/2 Pt/[0.6 Pt/0.9 Co/0.6 Ir]$_1$/2 MgO/1 Ta	
D	Sub./1.5 Ta/d Ir/1 CoFeB/2 MgO/1 Ta	d = 1,2,3,4,5,6,7,8 nm
E	Sub./1.5 Ta/7 Ir/0.9 Co/2 MgO/1 Ta	
F	Sub./3 Ta/2 Pt/1 Ir/0.9 Co/2 MgO/1 Ta	

and E is Co and amorphous Ta [31], respectively. (We do not have the information on the structure of the Co layer in films A–C as it is too thin to perform structural characterization.) All films possess sufficiently strong perpendicular magnetic anisotropy so that the magnetic easy axis points along the film normal (i.e., along the z axis). A summary of the film stacking is presented in Table I.

Optical lithography and Ar ion milling were used to form Hall bars from films A–C, E, and F. The width (w) and the distance (L) between the longitudinal voltage probes are $\sim$10 μm and $\sim$25 μm, respectively. Figure 2(a) shows an optical microscopy image of a typical Hall bar with the definition of the coordinate axis. A dc current is applied along the x axis: positive current is defined as current flow to $+x$. External magnetic fields were applied along the x, y, and z directions, referred to as H_x, H_y, and H_z, respectively. DMI, SOT, and SMR were evaluated using the patterned Hall bars. For reference film D, Hall bars with $w \sim 0.4$ mm and $L \sim 1.2$ mm were formed using a predefined shadow mask during the deposition process.

Magnetic properties of the films were studied using a vibrating sample magnetometer (VSM). The saturation magnetization (M_s) and the effective magnetic anisotropy energy ($K_{\rm eff}$) were estimated from the magnetic easy- and hard-axes hysteresis loops. The nominal FM layer thickness is used to calculate M_s. The X layer thickness (d) dependences of M_s and $K_{\rm eff}$ for films A and B are shown in the Supplemental Material [32] (Fig. S1). The results are interpolated to obtain the corresponding value of M_s and $K_{\rm eff}$ for the patterned devices made from films A and B. M_s and $K_{\rm eff}$ of reference films E and F are summarized in Table II.

III. EXPERIMENTAL RESULTS AND DISCUSSIONS

A. Spin-diffusion length of Ir

We first study the SMR [25–28] of reference film D [Sub./1.5 Ta/d Ir/1 CoFeB/2 MgO/1 Ta] to determine the spin-diffusion length of Ir. The longitudinal resistance R_{xx} of the Hall bar was measured while a constant magnitude magnetic field was applied to the sample. The relative angle (θ) between the magnetic field and the film normal was varied, as shown in the inset of Fig. 1(a). The magnetic field was rotated in the yz plane (current flow is along the x axis): under such circumstance, the resistance variation against θ provides information on the SMR [25–27]. The applied magnetic field was large enough ($\sim$3 T) to align the magnetic moment of the FM layer (CoFeB) along the magnetic field.

The inset of Fig. 1(b) shows the Ir layer thickness (d) variation of the sheet conductance [$L/(wR^z_{xx})$]. Except for the thinnest Ir layer film, the sheet conductance scales linearly with d. The slope of $L/(wR^z_{xx})$ vs d is proportional to the inverse of the Ir layer resistivity: we estimate the resistivity to be $\sim$19 $\mu\Omega$ cm. It is not clear what causes the deviation of the thinnest Ir layer film from the linear fitting: we infer that some degree of intermixing with Ta and/or CoFeB layers may influence the transport properties. The magnetic field angle (θ) dependence of R_{xx} is displayed in Fig. 1(a). Data are fitted with a sinusoidal function to obtain the resistance difference $\Delta R^{\rm SMR}_{xx}$ when the FM layer magnetization points along the y axis (R^y_{xx}) and the film normal (R^z_{xx}), i.e., $\Delta R^{\rm SMR}_{xx} = R^y_{xx} - R^z_{xx}$. The resistance ratio $\Delta R^{\rm SMR}_{xx}/R^z_{xx}$ is plotted as a function of d in Fig. 1(b). $|\Delta R^{\rm SMR}_{xx}/R^z_{xx}|$ increases with decreasing Ir layer thickness and shows the largest value at an Ir layer thickness

TABLE II. Summary of the saturation magnetization $M_{\rm s}$, the effective magnetic anisotropy energy $K_{\rm eff}$, DMI exchange field $H_{\rm DM}$, the DM exchange constant $|D|$, and the spin torque efficiency $\xi_{\rm DL}$ for [0.6 Pt/0.9 Co/d X]$_N$ multilayers (films A, B, C) and the reference films E and F. For films A and B, we take data from $d \sim 0.6$ nm so that the results can be compared to those of film C (note that $|D|$ saturates when $d >\sim 0.6$ nm).

ID unit	Stack	$M_{\rm s}$ (kA/m)	$K_{\rm eff}$ (10^5 J/m^3)	$H_{\rm DM}$ (T)	$\lvert D\rvert$ (mJ/m^2)	$\xi_{\rm DL}$
A	[0.6 Pt/0.9 Co/d Ir]$_3$ ($d \sim 0.6$ nm)	1060	7.9	0.08	0.4	0.08
B	[0.6 Pt/0.9 Co/d Cu]$_3$ ($d \sim 0.6$ nm)	1490	3.2	0.18	1.8	0.07
C	[0.6 Pt/0.9 Co/0.6 Ir]$_1$	1060[a]	4.7[b]	0.11	0.7	0.07
E	7 Ir/0.9 Co	910	2.3	0.22	1.6	0.01
F	2 Pt/1 Ir/0.9 Co	950	2.9	0.15	1.1	0.03

[a]$M_{\rm s}$ is assumed to be the same with that of film A (X = Ir, N = 3) with $d \sim 0.6$ nm.
[b]$K_{\rm eff}$ is obtained from $K_{\rm eff} = \mu_0 H_K M_s/2$ where the magnetic anisotropy field (H_K) was measured from the in-plane magnetic field dependence of the anomalous Hall resistance.

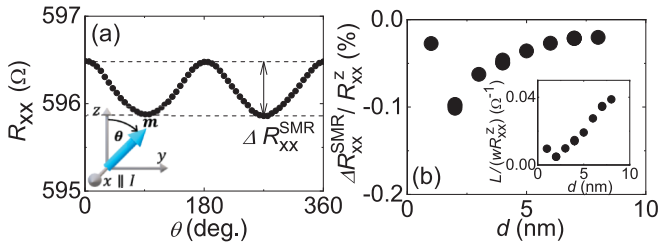

FIG. 1. (a) Longitudinal resistance R_{xx} of reference film D (Sub./1.5 Ta/2 Ir/1 CoFeB/2 MgO) plotted as a function of the angle θ between the magnetic field and the film normal (z axis). The applied magnetic field is 3 T. The inset shows the definition of the coordinate axis. (b) Spin Hall magnetoresistance ($\Delta R_{xx}^{SMR}/R_{xx}^{z}$) plotted as a function of the Ir layer thickness (d) for reference film D. The inset shows $L/(wR_{xx}^{z})$ vs d for the same film. The results presented were obtained using Hall bars with $L \sim 1.2$ mm and $w \sim 0.4$ mm.

of ∼2 nm. Based on the theory of SMR [26], the thickness at which $\Delta R_{xx}^{SMR}/R_{xx}^{z}$ takes a maximum is roughly two times the spin-diffusion length of the spin current generating layer. Although the thinnest Ir layer film exhibits a different resistivity from the other films, these results show that the spin-diffusion length of Ir is less than ∼1 nm. The combination of short spin-diffusion length and high conductivity makes Ir a good spin sink.

B. Current-induced shift of the anomalous Hall loop

The anomalous Hall resistance R_{xy} was measured against the out-of-plane field H_z under application of a dc bias current I_{DC} and an in-plane bias field H_x. Figure 2(b) shows exemplary R_{xy}–H_z loops for a Hall bar made of film C (X = Ir, $N = 1$, $d \sim 0.6$ nm) and $H_x = 0.2$ T, $I_{DC} = \pm 12$ mA. When positive (negative) current is applied, the center of the hysteresis loop shifts to negative (positive) H_z. The shift of the loop center with respect to $H_z = 0$ is defined as $-H_{eff}^{z}$. H_{eff}^{z} is plotted as a function of current density (J) in Fig. 2(c). We convert the bias current I_{DC} to J assuming that the majority of current flows uniformly in the conducting metallic layers (Pt, Co, Ir). (Taking into account the thickness-dependent resistivity of each layer changes the estimation of the SOT by at most ∼10%.) Since the resistivity of the thin Ta underlayer is nearly an order of magnitude larger than the conducting layers and the MgO/Ta capping layer is insulating (the top Ta layer is oxidized), current flow into these layers is neglected for all structures. As is evident, H_{eff}^{z} scales linearly with J. We thus fit H_{eff}^{z} vs J with a linear function. The slope of the fitted function H_{eff}^{z}/J is plotted against H_x in Fig. 2(d).

Following the analyses of Pai *et al.* [24], the H_x at which H_{eff}^{z}/J saturates [Fig. 2(d)] represents the DM exchange field H_{DM} and the saturation value of H_{eff}^{z}/J, which we will refer to as $H_{eff}^{z}/J|_{sat}$, is proportional to the spin torque efficiency ξ_{DL}, i.e., $H_{eff}^{z}/J|_{sat} = (\pi/2)(\hbar/2eM_s t_F)\xi_{DL}$ (see also Ref. [33]). $\hbar$ and e are the reduced Planck constant and the electric charge, respectively, M_s and t_F are the saturation magnetization and the thickness of the FM (Co) layer. Note that the sign of DMI (i.e., the magnetic chirality) cannot be determined from these measurements.

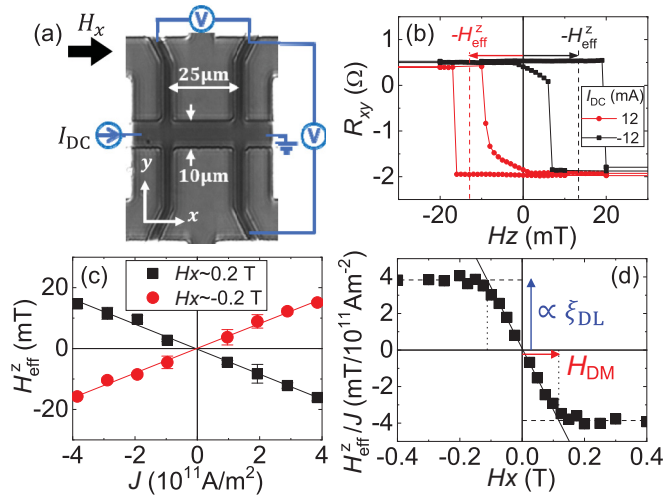

FIG. 2. (a) Optical micrograph of a representative Hall bar with the definition of the coordinate axis. (b) Anomalous Hall resistance (R_{xy}) vs H_z for two different dc currents ($I_{DC} = \pm 12$ mA) for film C (X = Ir, $N = 1$, $d \sim 0.6$ nm). The bias field along x (H_x) is fixed to ∼0.2 T. The definition of H_{eff}^{z} is schematically illustrated. (c) H_{eff}^{z} vs current density J for the same film with $H_x \sim \pm 0.2$ T. A linear function is fitted to the data to obtain the slope H_{eff}^{z}/J. The fitting results are shown by the solid lines. The error bars show the standard deviation of H_{eff}^{z} from repeated measurements. (d) The slope H_{eff}^{z}/J plotted as a function of the bias field H_x. H_{DM} and $H_{eff}^{z}/J|_{sat}$, which is proportional to ξ_{DL}, are extracted as schematically drawn (see text for the details).

C. Spin-orbit torque

The H_x dependence of H_{eff}^{z}/J for reference films E [Sub./1.5 Ta/7 Ir/0.9 Co/2 MgO/1 Ta] and F [Sub./3 Ta/2 Pt/1 Ir/0.9 Co/2 MgO/1 Ta] are shown in Figs. 3(a) and 3(b), respectively. For both films, the FM layer (Co) is sandwiched between an Ir underlayer and a MgO capping layer. The spin torque efficiency ξ_{DL} is estimated from $H_{eff}^{z}/J|_{sat}$: the values are listed in Table II. ξ_{DL} for reference film E is ∼0.01. A similar value was reported in Ref. [19]. Since the Ir layer thickness for reference film E is much larger than its spin-diffusion length, ξ_{DL} represents the bulk spin Hall angle of Ir (neglecting interfacial effects such as spin memory loss [34]). ξ_{DL} for reference film F is larger than film E due to the larger spin Hall effect of Pt placed below the Ir layer. As discussed below, the Ir layer tends to absorb spin current that diffuses in from neighboring layers, and thus ξ_{DL} of reference film F is likely to be smaller than that of Pt [30,35]. As the sign of

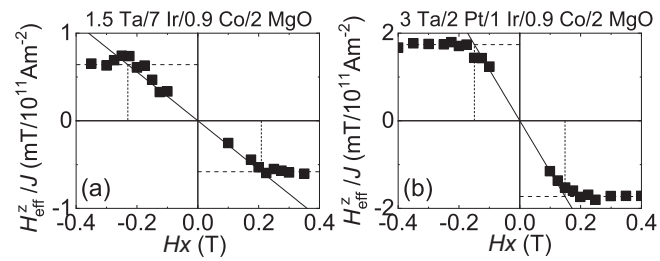

FIG. 3. H_{eff}^{z}/J vs H_x for reference films (a) E [Sub./1.5 Ta/7 Ir/0.8 Co/2 MgO/1 Ta] and (b) F [Sub./3 Ta/2 Pt/1 Ir/0.9 Co/2 MgO/1 Ta].

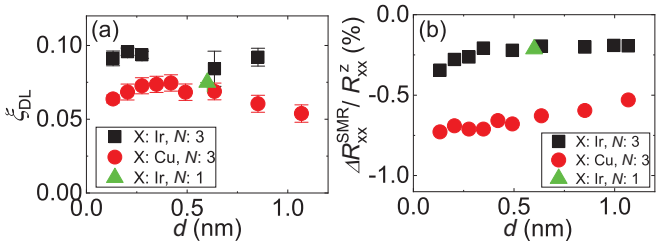

FIG. 4. (a) Spin torque efficiency ξ_{DL} and (b) spin Hall magnetoresistance $\Delta R_{xx}^{SMR}/R_{xx}^{z}$ plotted as a function of the X layer thickness (d) for films A–C ($[0.6\,\mathrm{Pt}/0.9\,\mathrm{Co}/d\,X]_N$ multilayers). Black squares: film A ($X = \mathrm{Ir}$, $N = 3$); red circles: film B ($X = \mathrm{Cu}$, $N = 3$); and green triangles: film C ($X = \mathrm{Ir}$, $N = 1$). The error bars in (a) represent standard deviation of the data used to obtain ξ_{DL} from the plot of H_{eff}^{z}/J vs H_x with $|H_x| > |H_{DM}|$ [see, e.g., Fig. 2(d)]. The error bars for the results shown in (b) are smaller than the symbol size.

$H_{\mathrm{eff}}^{z}/J|_{\mathrm{sat}}$ is the same for films E and F, we consider that the spin Hall angles of Ir and Pt possess the same sign.

The spin torque efficiencies ξ_{DL} for films A–C ($[0.6\,\mathrm{Pt}/0.9\,\mathrm{Co}/d\,X]_N$ multilayers) are plotted as a function of X (=Ir and Cu) layer thickness (d) in Fig. 4(a). Black squares, red circles, and green triangles correspond to ξ_{DL} of film A ($X = \mathrm{Ir}$, $N = 3$), film B ($X = \mathrm{Cu}$, $N = 3$), and film C ($X = \mathrm{Ir}$, $N = 1$), respectively. Comparison of the results from films A and B ($X = \mathrm{Ir}$, Cu, $N = 3$) shows that ξ_{DL} for $X = \mathrm{Cu}$ multilayers is smaller than that of $X = \mathrm{Ir}$ multilayers. To reveal the role of the X layer on ξ_{DL} more precisely, the SMR of films A–C was measured. $\Delta R_{xx}^{SMR}/R_{xx}^{z}$ is plotted as a function of d in Fig. 4(b). Although the yz plane magnetoresistance may contain contributions from other sources, here we assume the relative magnitude is comparable since the Co layer is sufficiently thin (note the anomalous SMR emerges for thicker Co films [29,36–39]) and its thickness is the same for both multilayers. For both systems, $|\Delta R_{xx}^{SMR}/R_{xx}^{z}|$ decreases with increasing d. However, $|\Delta R_{xx}^{SMR}/R_{xx}^{z}|$ is significantly smaller for $X = \mathrm{Ir}$ multilayers (film A) compared to that of $X = \mathrm{Cu}$ (film B). As the spin accumulation at interfaces is proportional to the spin torque efficiency ξ_{DL}, these results are in contrast to the results shown in Fig. 4(a). Note that the single-repeat multilayer ($N = 1$, $X = \mathrm{Ir}$, film C) shows similar results with those of the corresponding $N = 3$ repeated stacks (film A).

The contradictory results of ξ_{DL} [Fig. 4(a)] and SMR [Fig. 4(b)] can be accounted for qualitatively if we assume the Ir layer acts as a spin sink and hinders spin transmission across the layer. Illustrations of the electron spin transport and the resulting SOT in the unit structure of the multilayers ($N > 1$) are depicted in Fig. 5. Figures 5(a) and 5(c) show the spin accumulation $\vec{\sigma}$ at the top and bottom interfaces of the Co layer due to the spin Hall induced spin current generated from the top and bottom Pt layers in $X = \mathrm{Cu}$ and Ir multilayers, respectively. Here we have assumed that Cu and Ir generate negligible spin current (see Table II for ξ_{DL} of Ir). Since the bottom Pt/Co interface is the same for both multilayers, the spin torque efficiency depends on the amount of spin accumulation at the top Co interface. For $X = \mathrm{Cu}$ [Fig. 5(a)], the spin current from the top Pt layer (on top of Cu) traverses the Cu layer and impinges on the Co layer, resulting in spin

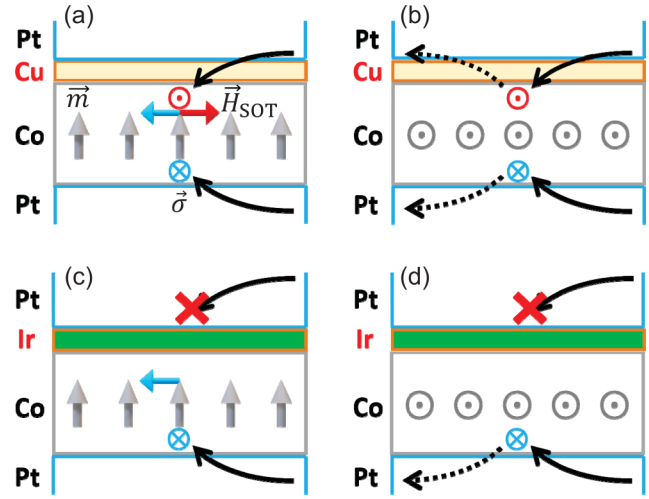

FIG. 5. (a)–(d) Illustration of spin transport in the $[\mathrm{Pt}/\mathrm{Co}/X]_N$ multilayers ($X = \mathrm{Ir}$, Cu, N>1). $\vec{m}$, $\vec{\sigma}$ and $\vec{H}_{SOT}$ indicate the magnetization direction of the Co layer, spin polarization of the conduction electrons diffusing in from the Pt layers via the spin Hall effect, and the spin-orbit effective field acting on the magnetic moments. $\vec{H}_{SOT}$ associated with the spin current from the top and bottom Pt layers are illustrated by the red and blue arrows, respectively. (a),(b) $X = \mathrm{Cu}$ and (c),(d) $X = \mathrm{Ir}$. The Ir layer is assumed to absorb spin current that diffuses in from the top Pt layer. Co magnetization points along the film normal, i.e., along z, for (a),(c), and along the film plane, i.e., along y, for (b),(d). For the latter, charge current due to the inverse spin Hall effect is depicted by the dotted lines.

accumulation at the Co/Cu interface. Since the spin currents from the top and bottom Pt layers point to opposite directions, the net torque on the magnetic moments will work against each other. ξ_{DL} of $X = \mathrm{Ir}$ [Fig. 5(c)] is thus larger than that of $X = \mathrm{Cu}$ since the Ir layer absorbs the spin current from the Pt layer due to its short spin-diffusion length, which results in reduction of the torque compensation.

The SMR, on the other hand, is proportional to the spin accumulation at the FM/HM interface, but the sign of $\vec{\sigma}$ does not influence the overall magnitude: i.e., the SMR scales with the square of the spin Hall angle [26]. The spin accumulation at the top and bottom interfaces therefore contributes to the SMR in a constructive manner, unless the FM layer is too thin to cause cross talk of spin accumulation at the top and bottom interfaces. Assuming negligible cross talk, the larger SMR for the $X = \mathrm{Cu}$ multilayer can be accounted for if the degree of spin accumulation at the top interface is larger [see Figs. 5(a)–5(d)]. The smaller SMR for the $X = \mathrm{Ir}$ multilayers can be attributed to absorption of the spin current at the Ir layer diffusing in from the top Pt layer. This observation is consistent with the results of $N = 1$ ($X = \mathrm{Ir}$) multilayers (film C): both ξ_{DL} and the SMR take similar value with those of the $N = 3$ multilayers, suggesting that the Pt layer on top of the Ir layer for the $N = 3$ multilayer has little influence on the SOT/spin accumulation.

D. Dzyaloshinskii-Moriya interaction

As schematically shown in Fig. 2(d), H_{DM} is obtained by first fitting H_{eff}^{z}/J vs H_x with a linear function in appropriate ranges of H_x around $H_x \sim 0$. We then look for the intersection

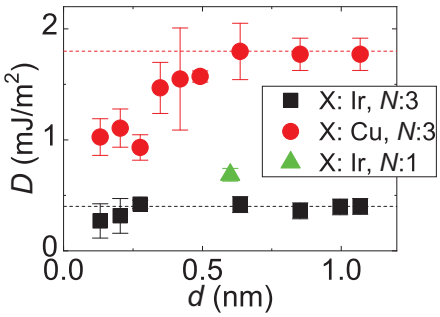

FIG. 6. The DM exchange constant $|D|$ vs X layer thickness (d) for films A–C ($[0.6\,\mathrm{Pt}/0.9\,\mathrm{Co}/d\,X]_N$ multilayers). Black squares: film A ($X = \mathrm{Ir}$, $N = 3$); red circles: film B ($X = \mathrm{Cu}$, $N = 3$); and green triangles: film C ($X = \mathrm{Ir}$, $N = 1$). Broken lines, which are a guide to the eye, illustrate values of $|D|$ with large d. The error bars represent the range of H_{DM} when the range of linear fitting to H_{eff}^{z}/J vs H_x is varied.

of the fitted linear line with the saturated value of H_{eff}^{z}/J and take the x coordinate of the intersection as H_{DM}. The DM exchange constant D is calculated from H_{DM} using the relation $|D| = \mu_0 M_s H_{\mathrm{DM}} \Delta$. Here, A is the exchange stiffness constant and $\Delta = \sqrt{A/K_{\mathrm{eff}}}$. We assume $A = 15$ pJ/m for all films studied [40,41]. The obtained $|D|$ for films A, B, and C ($[0.6\,\mathrm{Pt}/0.9\,\mathrm{Co}/d\,X]_N$) is plotted as a function of X layer thickness (d) in Fig. 6. For films A and B, $|D|$ increases with increasing d until it saturates at a certain d. Upon saturation, we find $|D| \sim 1.8\,\mathrm{mJ/m^2}$ for $X = \mathrm{Cu}$ and $|D| \sim 0.4\,\mathrm{mJ/m^2}$ for $X = \mathrm{Ir}$. Interestingly, $|D|$ is significantly larger for $X = \mathrm{Cu}$ (similar results have been reported in Ref. [42]). If we assume the DMI at the Co/Cu interface is negligible, the results from $X = \mathrm{Cu}$ (film B) suggest the DMI of Pt/Co interface is $|D| \sim 1.8\,\mathrm{mJ/m^2}$. The fact that $|D|$ is smaller for $X = \mathrm{Ir}$ multilayers (film A) indicates that the DMI of the Co/Ir interface has the opposite sign from that of Pt/Co interface, similar to the results reported in Refs. [19,20,43–45]. (In terms of the DMI with the same stacking order, the Ir/Co interface and Pt/Co interface possess the same sign.) Assuming that DMI at the top and bottom interfaces of a FM layer are additive, we estimate $|D| \sim 1.4$ or $2.2\,\mathrm{mJ/m^2}$ for the Ir/Co interface. (Since the sign of D cannot be determined from these measurements, $|D|$ can be either 1.4 or $2.2\,\mathrm{mJ/m^2}$ to account for the values obtained for the $X = \mathrm{Cu}$ and $X = \mathrm{Ir}$ multilayers.) The DMI of $N = 1$, $X = \mathrm{Ir}$ multilayer (film C), shown by the green triangle in Fig. 6, suggest that the number of stacking does not necessarily influence the DMI.

Recently, it was reported that the DMI of the Co/Ir interface may depend on its structure: in particular, the sign of DMI can change between fcc-based and hcp-based Ir structures [18]. These studies suggest that the DMI of the Ir/Co (or Co/Ir) interface can be influenced by the layer underneath it which controls the growth mode. The reference films E and F possess structures in which the underlayer of Ir is different from that of the multilayers (films A–C). The underlayer is Ta and Pt for reference films E and F, respectively, whereas Co is deposited before Ir for the multilayers. The DMI values of the reference films E and F, obtained from the results presented in Fig. 3, are summarized in Table II. Interestingly, $|D|$ of reference film E (Ir grown on Ta) exhibits similar magnitude ($\sim 1.6\,\mathrm{mJ/m^2}$) with that of the Co/Ir interface in the multilayers. We find a smaller $|D|$ for reference film F (Ir on Pt): the origin of the difference in DMI between the reference films E and F is not clear.

We also studied current-induced motion of magnetic domain walls in patterned wires made of films with stacking similar to those of reference films E and F. We find the domain walls move along the current flow in all cases, in agreement with the results reported in Ref. [19]. (Due to strong pinning, it is difficult to move the domain walls along the wire smoothly, which hinders accurate evaluation of the wall velocity.) Since the effective spin Hall angle of Ir has the same sign as that of Pt, these results suggest that the sign of the DMI at the Ir/Co interface is the same as that of the Pt/Co interface. Together with the results presented in Table II, we conclude that the Ir/Co interface possesses a DMI that has the same sign as that of Pt/Co and the magnitude is similar.

IV. SUMMARY

We have studied the spin torque efficiency and the Dzyaloshinskii-Moriya interaction (DMI) at the Co and Ir interface using $[\mathrm{Pt/Co}/X]_N$ multilayers ($X = \mathrm{Cu}$ and Ir) and Ir/Co, Pt/Ir/Co reference films. The current-induced shift of the anomalous Hall hysteresis loops is used to evaluate the spin torque efficiency and the Dzyaloshinskii-Moriya interaction. We find that Ir possesses a positive and relatively small spin Hall angle of ~ 0.01 (same sign with that of Pt), and its spin-diffusion length is less than ~ 1 nm. Due to its high electrical conductivity and short spin-diffusion length, the Ir layer acts as a good spin sink. Such characteristics of Ir can be used to break flows of spin current that will otherwise reduce the spin torque efficiency. The DMI at the interface of Co and Ir is found to be of similar magnitude with that of the Co and Pt interface. We find the magnitude of the DM exchange constant at the Ir/Co (and Co/Ir) interface to be ~ 1.4–$2.2\,\mathrm{mJ/m^2}$. The sign of the DM exchange constant for Pt/Co and Ir/Co interfaces turns out to be the same, leading to a reduced DMI for the Pt/Co/Ir multilayers. These results show that Ir can be used as an efficient spin-absorbing layer as well as a source of DMI.

ACKNOWLEDGMENTS

The authors thank K. Yawata for technical support. This work was partly supported by JSPS Grant-in-Aid for Scientific Research (Grant No. 16H03853), Specially Promoted Research (Grant No. 15H05702), Casio Science Foundation, and the Center of Spintronics Research Network of Japan. Y.-C.L. is supported by a JSPS International Fellowship for Research in Japan (Grant No. JP17F17064).

[1] I. E. Dzyaloshinskii, Sov. Phys. JETP **19**, 960 (1964).

[2] T. Moriya, Phys. Rev. **120**, 91 (1960).

[3] A. Fert, V. Cros, and J. Sampaio, Nat. Nanotechnol. **8**, 152 (2013).

[4] K.-S. Ryu, L. Thomas, S.-H. Yang, and S. Parkin, Nat. Nanotechnol. **8**, 527 (2013).

[5] S. Emori, U. Bauer, S.-M. Ahn, E. Martinez, and G. S. D. Beach, Nat. Mater. **12**, 611 (2013).

[6] J. Torrejon, J. Kim, J. Sinha, S. Mitani, M. Hayashi, M. Yamanouchi, and H. Ohno, Nat. Commun. **5**, 4655 (2014).

[7] G. Chen, T. Ma, A. T. N'Diaye, H. Kwon, C. Won, Y. Wu, and A. K. Schmid, Nat. Commun. **4**, 2671 (2013).

[8] C. Moreau Luchaire, C. Moutafis, N. Reyren, J. Sampaio, C. A. F. Vaz, N. Van Horne, K. Bouzehouane, K. Garcia, C. Deranlot, P. Warnicke, P. Wohlhüter, J. M. George, M. Weigand, J. Raabe, V. Cros, and A. Fert, Nat. Nano **11**, 444 (2016).

[9] S. Woo, K. Litzius, B. Kruger, M.-Y. Im, L. Caretta, K. Richter, M. Mann, A. Krone, R. M. Reeve, M. Weigand, P. Agrawal, I. Lemesh, M.-A. Mawass, P. Fischer, M. Klaui, and G. S. D. Beach, Nat. Mater. **15**, 501 (2016).

[10] O. Boulle, J. Vogel, H. Yang, S. Pizzini, D. de Souza Chaves, A. Locatelli, T. O. Menteş, A. Sala, L. D. Buda-Prejbeanu, O. Klein, M. Belmeguenai, Y. Roussigné, A. Stashkevich, S. M. Chérif, L. Aballe, M. Foerster, M. Chshiev, S. Auffret, I. M. Miron, and G. Gaudin, Nat. Nano **11**, 449 (2016).

[11] A. Soumyanarayanan, M. Raju, A. L. G. Oyarce, A. K. C. Tan, M. Y. Im, A. P. Petrovic, P. Ho, K. H. Khoo, M. Tran, C. K. Gan, F. Ernult, and C. Panagopoulos, Nat. Mater. **16**, 898 (2017).

[12] K. W. Kim, H. W. Lee, K. J. Lee, and M. D. Stiles, Phys. Rev. Lett. **111**, 216601 (2013).

[13] H. Yang, A. Thiaville, S. Rohart, A. Fert, and M. Chshiev, Phys. Rev. Lett. **115**, 267210 (2015).

[14] A. Belabbes, G. Bihlmayer, F. Bechstedt, S. Blugel, and A. Manchon, Phys. Rev. Lett. **117**, 247202 (2016).

[15] T. Kikuchi, T. Koretsune, R. Arita, and G. Tatara, Phys. Rev. Lett. **116**, 247201 (2016).

[16] A. Hrabec, N. A. Porter, A. Wells, M. J. Benitez, G. Burnell, S. McVitie, D. McGrouther, T. A. Moore, and C. H. Marrows, Phys. Rev. B **90**, 020402(R) (2014).

[17] M. Perini, S. Meyer, B. Dupe, S. von Malottki, A. Kubetzka, K. von Bergmann, R. Wiesendanger, and S. Heinze, Phys. Rev. B **97**, 184425 (2018).

[18] G. J. Vida, E. Simon, L. Rozsa, K. Palotas, and L. Szunyogh, Phys. Rev. B **94**, 214422 (2016).

[19] K. S. Ryu, S. H. Yang, L. Thomas, and S. S. P. Parkin, Nat. Commun. **5**, 3910 (2014).

[20] K. Shahbazi, J.-V. Kim, H. T. Nembach, J. M. Shaw, A. Bischof, M. D. Rossell, V. Jeudy, T. A. Moore, and C. H. Marrows, Phys. Rev. B **99**, 094409 (2019).

[21] I. M. Miron, K. Garello, G. Gaudin, P. J. Zermatten, M. V. Costache, S. Auffret, S. Bandiera, B. Rodmacq, A. Schuhl, and P. Gambardella, Nature (London) **476**, 189 (2011).

[22] L. Liu, C.-F. Pai, Y. Li, H. W. Tseng, D. C. Ralph, and R. A. Buhrman, Science **336**, 555 (2012).

[23] A. Manchon, H. C. Koo, J. Nitta, S. M. Frolov, and R. A. Duine, Nat. Mater. **14**, 871 (2015).

[24] C.-F. Pai, M. Mann, A. J. Tan, and G. S. D. Beach, Phys. Rev. B **93**, 144409 (2016).

[25] H. Nakayama, M. Althammer, Y. T. Chen, K. Uchida, Y. Kajiwara, D. Kikuchi, T. Ohtani, S. Geprags, M. Opel, S. Takahashi, R. Gross, G. E. W. Bauer, S. T. B. Goennenwein, and E. Saitoh, Phys. Rev. Lett. **110**, 206601 (2013).

[26] Y. T. Chen, S. Takahashi, H. Nakayama, M. Althammer, S. T. B. Goennenwein, E. Saitoh, and G. E. W. Bauer, Phys. Rev. B **87**, 144411 (2013).

[27] M. Althammer, S. Meyer, H. Nakayama, M. Schreier, S. Altmannshofer, M. Weiler, H. Huebl, S. Geprägs, M. Opel, R. Gross, D. Meier, C. Klewe, T. Kuschel, J.-M. Schmalhorst, G. Reiss, L. Shen, A. Gupta, Y.-T. Chen, G. E. W. Bauer, E. Saitoh, and S. T. B. Goennenwein, Phys. Rev. B **87**, 224401 (2013).

[28] J. Kim, P. Sheng, S. Takahashi, S. Mitani, and M. Hayashi, Phys. Rev. Lett. **116**, 097201 (2016).

[29] M. Kawaguchi, D. Towa, Y. C. Lau, S. Takahashi, and M. Hayashi, Appl. Phys. Lett. **112**, 202405 (2018).

[30] C.-F. Pai, Y. Ou, L. H. Vilela-Leao, D. C. Ralph, and R. A. Buhrman, Phys. Rev. B **92**, 064426 (2015).

[31] J. Liu, T. Ohkubo, S. Mitani, K. Hono, and M. Hayashi, Appl. Phys. Lett. **107**, 232408 (2015).

[32] See Supplemental Material at http://link.aps.org/supplemental/10.1103/PhysRevB.99.134421 for the magnetic properties of films A and B.

[33] A. Thiaville, S. Rohart, E. Jue, V. Cros, and A. Fert, Europhys. Lett. **100**, 57002 (2012).

[34] J. C. Rojas-Sanchez, N. Reyren, P. Laczkowski, W. Savero, J. P. Attane, C. Deranlot, M. Jamet, J. M. George, L. Vila, and H. Jaffres, Phys. Rev. Lett. **112**, 106602 (2014).

[35] W. Zhang, W. Han, X. Jiang, S.-H. Yang, and S. S. P. Parkin, Nat. Phys. **11**, 496 (2015).

[36] W. Gil, D. Gorlitz, M. Horisberger, and J. Kotzler, Phys. Rev. B **72**, 134401 (2005).

[37] A. Kobs, S. Hesse, W. Kreuzpaintner, G. Winkler, D. Lott, P. Weinberger, A. Schreyer, and H. P. Oepen, Phys. Rev. Lett. **106**, 217207 (2011).

[38] A. Kobs and H. P. Oepen, Phys. Rev. B **93**, 014426 (2016).

[39] L. K. Zou, Y. Zhang, L. Gu, J. W. Cai, and L. Sun, Phys. Rev. B **93**, 075309 (2016).

[40] H. F. Ding, W. Wulfhekel, and J. Kirschner, Europhys. Lett. **57**, 100 (2002).

[41] R. Moreno, R. F. L. Evans, S. Khmelevskyi, M. C. Muñoz, R. W. Chantrell, and O. Chubykalo-Fesenko, Phys. Rev. B **94**, 104433 (2016).

[42] S. Schlotter, P. Agrawal, and G. S. D. Beach, Appl. Phys. Lett. **113**, 092402 (2018).

[43] P. M. Shepley, H. Tunnicliffe, K. Shahbazi, G. Burnell, and T. A. Moore, Phys. Rev. B **97**, 134417 (2018).

[44] D. Khadka, S. Karayev, and S. X. Huang, J. Appl. Phys. **123**, 123905 (2018).

[45] N. H. Kim, J. Jung, J. Cho, D. S. Han, Y. X. Yin, J. S. Kim, H. J. M. Swagten, and C. Y. You, Appl. Phys. Lett. **108**, 142406 (2016).